Journal of Molecular Structure 1046 (2013) 147–152

Contents lists available at SciVerse ScienceDirect

Journal of Molecular Structure

journal homepage: www.elsevier.com/locate/molstruc

Synthesis, structure, theoretical calculations and biological activity of sulfonate active ester new derivatives

Mohamed Ghazzali [a,*], Sherine A.N. Khattab [b], Yasser A. Elnakady [c], Fahd A. Al-Mekhlafi [c], Khalid Al-Farhan [a], Ayman El-Faham [a,b]

[a] Department of Chemistry, College of Science, King Saud University, P.O. 2455, 11451 Riyadh, Saudi Arabia
[b] Department of Chemistry, Faculty of Science, Alexandria University, P.O. Box 426, Ibrahimia, 21321 Alexandria, Egypt
[c] Department of Zoology, College of Science, King Saud University, P.O. Box 2455, Riyadh 11451, Saudi Arabia

HIGHLIGHTS

- Three structural determinations of new active ester derivatives are presented.
- Intermolecular interactions were investigated by *DFT-B3LYP* theory.
- Biological activities were studied for selected compounds.

GRAPHICAL ABSTRACT

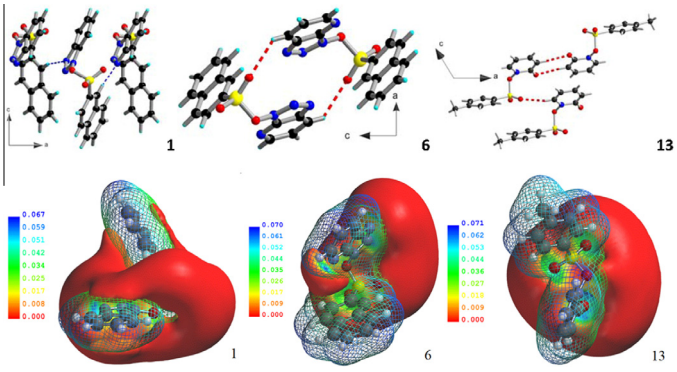

ARTICLE INFO

Article history:
Received 6 February 2013
Received in revised form 19 March 2013
Accepted 11 April 2013
Available online 25 April 2013

Keywords:
Sulfonate active ester
N-protected amino acid
X-ray single crystal diffraction
Biological activity
DFT/MP2 calculations

ABSTRACT

A series of naphthyl and tolyl sulfonate ester were synthesized and characterized by H NMR. X-ray single crystal diffraction experiments established the molecular structure of three new sulfonate esters derivatives, and spectral data agree with these in solution. The observed hydrogen bonding is discussed on the basis of crystal structural analyses and *DFT/MP2* geometry optimization quantum calculations. Antimicrobial activities were screened for selected compounds against three human cancer cell lines and Mosquito *Culex pipiens* larvae.

1. Introduction

The active esters are well known precursors in peptide bond reaction for both liquid- and solid-state synthesis [1,2]. An important step in peptide bond formation is the development of *N*-protected amino acid derivatives that are reactive enough to combine with amine groups when both are mixed. The *so*-called peptide coupling reagents are then responsible for activation of amino acids during the condensation step [3]. A major class of peptide coupling reagents is based on sulfonate ester derivatives of both 1-hydroxy benzotriazole, abbreviated afterwards as HOBt (**1**–**5** in Fig. 1) and 7-aza-1-hydroxy benzotriazole, abbreviated afterwards as HOAt (**6**–**10** in Fig. 1) [4]. The reactivity of such sulfonate esters was shown to be directly related to the presence of

* Corresponding author. Tel.: +966 14673734.
E-mail addresses: mghazzali@ksu.edu.sa, m.ghazzali@gmail.com (M. Ghazzali).

0022-2860/$ - see front matter © 2013 Elsevier B.V. All rights reserved.
http://dx.doi.org/10.1016/j.molstruc.2013.04.025

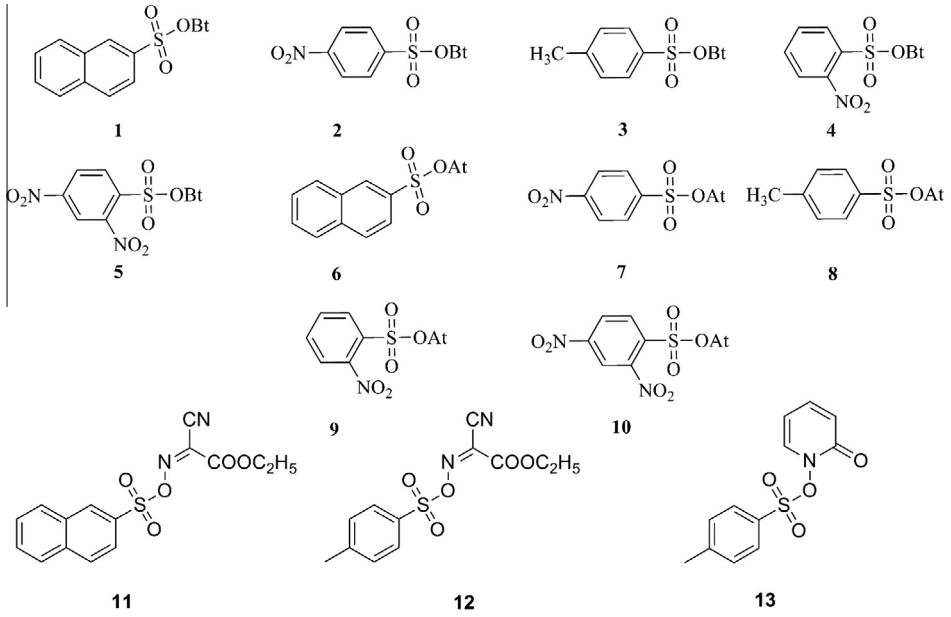

Fig. 1. Library of sulfonate active esters derived from HOBt (**1**–**5**), HOAt (**6**–**10**), Ethyl cyanoglyoxylate-2-oxime **11**, **12** and 1-hydroxypyridin-2-one **13**.

electron withdrawing substituents in both benzotriazole and sulfonate moieties [5].

However, the use of sulfonate esters are showing a scarce practice, since it is depending on the basicity of the amine component, while the *in situ* coupling method *via* the active ester intermediate is often compromised with a formation of sulfonamide byproduct [6]. Because of the explosive character of HOBt and it derivatives [7], one of us recently reported [8] the synthesis of sulfonate esters based on ethyl cyanoglyoxylate-2-oxime **11** and **12** as well 1-hydroxy-2-pyridinone **13** (Fig. 1) as new coupling agents. These derivatives showed some advantages over those of HOBt or HOAt in terms of yield, racemization-free reactivity with byproduct minimization. We are reporting here the synthesis, spectral characterization and molecular structure elucidation of three new sulfonate ester derivatives, evincing the *O*-form configuration of synthesized esters. We are extending the work to the structural and theoretical calculations of intermolecular interactions, existing in the solid phase of these compounds. The biological activity studies of some selected derivatives showed a moderate anti-proliferative effect against human cancer cell line SW756 for two compounds, while one derivative showed a strong growth inhibition for mosquito *Culex pipiens* 4th instar larvae.

2. Experimental

Melting points were measured by Mel-Temp apparatus. NMR spectra were recorded on a 500 MHz JEOL spectrophotometer. Chemical shifts relative to TMS internal reference are reported in δ-units.

2.1. General method for the synthesis of sulfonate esters

Adopting a method reported earlier [9], 5 mmol suspension of either 1-hydroxy benzotriazole or 7-aza-1-hydroxy benzotriazole or ethyl 2-cyano-2-(hydroxyimino)acetate or 1-hydroxypyridin-2(1*H*)-one in 30 mL of anhydrous CH_2Cl_2 was added to 5 mmol of triethylamine with magnetic stirring. The resulting clear yellow solution was cooled in an ice bath under N_2 atmosphere and treated slowly with one equivalent of 4-tosyl chloride or 2-naphthalenesulfonyl chloride. The reaction mixture was stirred at 0 °C for 30 min and then at room temperature for 2 h. After dilution with 30 mL of CH_2Cl_2, the organic phase was washed with water and dried over anhydrous Na_2SO_4. After solvent evaporation, the residue was recrystallized from CH_2Cl_2/hexane to give the corresponding sulfonate esters.

2.1.1. 1H-benzo[d][1-3]triazol-1-yl naphthalene-2-sulfonate ***1***

Colorless crystals in yield 80%, mp 128–129 °C, ^{1}H NMR (500 MHz, $CDCl_3$) 7.43 (t, 1H, Ar–H, *J* = 8.4 Hz), 7.57 (t, 1H, Ar–H, *J* = 7.7 Hz), 7.65 (t, 2H, Ar–H, *J* = 8.4 Hz), 7.75 (t, 1H, Ar–H, *J* = 8.4 Hz), 7.88–8.00 (m, 4H, Ar–H), 8.07 (d, 1H, Ar–H, *J* = 8.4 Hz), 8.45 (s, 1H, Ar–H). ^{13}C NMR (125 MHz, $CDCl_3$): 109.57, 120.41, 123.16, 125.46, 128.31, 128.41, 128.85, 128.98, 129.45, 129.87, 130.41, 130.81, 131.95, 132.81, 136.46, 143.80.

2.1.2. 1H-benzo[d][1,2,3]triazol-1-yl 4-methylbenzene sulfonate ***3***

Colorless crystals in yield 79%, mp 80–81 °C, ^{1}H NMR (500 MHz, $CDCl_3$): 2.52 (s, 3H, CH_3), 7.38–7.44 (m, 3H, Ar–H), 7.57 (t, 1H, Ar–H, *J* = 7.7 Hz), 7.62 (d, 1H, Ar–H, *J* = 8.6 Hz), 7.76 (d, 2H, Ar–H, *J* = 8.6 Hz), 7.99 (d, 1H, Ar–H, *J* = 8.6 Hz). ^{13}C NMR (125 MHz, $CDCl_3$): 22.08, 109.61, 120.35, 125.39, 127.14, 128.83, 129.16, 129.37, 129.90, 130.60, 143.01, 148.12.

2.1.3. 3H-[1,2,3]triazolo[4,5-b]pyridin-3-yl naphthalene-2-sulfonate ***6***

colorless crystals in yield 85%, mp 141–143 °C, ^{1}H NMR (500 MHz, $CDCl_3$): 7.43 (dd, 1H, Ar–H, *J* = 8.4, 4.6 Hz), 7.67 (t, 1H, Ar–H, *J* = 8.4 Hz), 7.75 (t, 1H, Ar–H, *J* = 8.4 Hz), 7.96–7.99 (m, 3H, Ar–H), 8.08 (d, 1H, Ar–H, *J* = 8.4 Hz), 8.36 (d, 1H, Ar–H, *J* = 9.2 Hz), 8.54 (s, 1H, Ar–H), 8.71 (d, 1H, Ar–H, *J* = 5.4 Hz). ^{13}C NMR (125 MHz, $CDCl_3$): 121.36, 123.30, 128.28, 128.36, 129.52, 129.57, 129.86, 130.33, 130.75, 131.97, 132.80, 134.53, 136.44, 152.45.

2.1.4. 3H-[1,2,3]triazolo[4,5-b]pyridin-3-yl 4-methylbenzene sulfonate ***8***

Colorless crystals in yield 76%, mp 131–133 °C, ^{1}H NMR (500 MHz, $CDCl_3$): 2.51 (s, 3H, CH_3), 7.41–7.45 (m, 3H, Ar–H), 7.87 (d, 2H, Ar–H, *J* = 7.6 Hz), 8.38 (d, 1H, Ar–H, *J* = 8.4 Hz), 8.77 (dd, 1H, Ar–H, *J* = 4.6, 1.6 Hz). ^{13}C NMR (125 MHz, $CDCl_3$): 22.13, 121.37, 129.53, 129.65, 129.98, 130.85, 134.55, 140.65, 148.05, 152.50.

2.1.5. Ethyl 2-cyano-2-(naphthalen-2-ylsulfonyloxyimino) acetate ***11***

Colorless crystals, 1.53 g (92%), mp 94–95 °C; ^{1}H NMR (500 MHz, $CDCl_3$): 1.35 (t, 3H, CH_3, J = 7.7 Hz), 4.38 (quart, 2H, CH_2, J = 7.7 Hz), 7.69, 7.75 (2t, 2H, Ar–H, J = 7.7 Hz), 7.95–7.97 (m, 2H, Ar–H), 8.03 (d, 1H, Ar–H, J = 2.3 Hz), 8.05 (d, 1H, Ar–H, J = 3.8 Hz), 8.68 (s, 1H, Ar–H). ^{13}C NMR (125 MHz, $CDCl_3$): 13.98, 64.69, 106.19, 123.14, 128.22, 128.37, 129.84, 130.00, 130.09, 130.58, 131.46, 131.96, 132.35, 155.94.

2.1.6. Ethyl 2-cyano-2-(tosyloxyimino) acetate ***12***

Colorless crystals in yield 85%, mp 64–65 °C. ^{1}H NMR (500 MHz, $CDCl_3$): 1.37 (t, 3H, CH_3, J = 6.9 Hz), 2.48 (s, 3H, CH_3), 4.40 (quart, 2H, CH_2, J = 6.9 Hz), 7.40 (d, 2H, Ar–H, J = 7.6 Hz), 7.92 (d, 2H, Ar–H, J = 7.6 Hz). ^{13}C NMR (125 MHz, $CDCl_3$): 14.00, 22.00, 64.66, 106.20, 129.64, 130.18, 130.36, 131.26, 147.39, 156.02.

2.1.7. 2-Oxopyridin-1(2H)-yl 4-methylbenzene sulfonate ***13***

Colorless crystals in yield 78%, mp 92–94 °C, ^{1}H NMR (500 MHz, $CDCl_3$): 2.47 (s, 3H, CH_3), 6.15 (dt, 1H, Ar–H, J = 6.4, 1.6 Hz), 6.51 (dd, 1H, Ar–H, J = 9.2, 1.6 Hz), 7.29 (m, 1H, Ar–H), 7.37 (d, 2H, Ar–H, J = 8.0 Hz), 7.59 (dd, 1H, Ar–H, J = 7.2, 2.0 Hz), 7.89 (d, 2H, Ar–H, J = 8.4 Hz). ^{13}C NMR (125 MHz, $CDCl_3$): 22.19, 105.32, 123.41, 130.01, 130.07, 130.09, 130.14, 130.19, 130.67, 137.16, 139.60, 147.44, 157.04.

3. X-ray single crystal diffraction

Suitable single crystals of compounds **1, 6** and **13** were selected, glued and mounted onto thin glass capillary. Diffraction data were collected using a Rigaku *R*-axis SPIDER diffractometer equipped with imaging plate area detector utilizing Mo Kα radiation (λ = 0.71075 Å) with graphite monochromator. The data were collected using ω-scans at a temperature of 294 ± 2 K to a maximum 2θ of 55.0°. Preliminary orientation matrices, unit cell determination, data reduction and absorption correction were performed using CrystalClear package [10]. The data were empirically corrected for Lorentz and polarization effects. Structures were solved by direct methods and refined by full-matrix least squares on all $|F^2|$ data using SHELX package [11]. Hydrogen atoms were isotropically refined and constrained to ideal geometry, using their appropriate riding model and non-hydrogen atoms were anisotropically refined. The crystallographic descriptive figures were created using DIAMOND package [12]. Crystallogrpahic data are summarized in Table 1.

4. Theoretical calculations

The *ab initio DFT* quantum calculations for **1**, **6** and **13** were calculated with SPARTAN08 package [13]. The starting *z*-matrices were truncated from X-ray derived coordinates and used without geometrical constraints. The geometry optimizations were performed at ground state by Hartree–Fock 6-31G* theory. The Hessians analysis shows only non-imaginary frequencies. The density was calculated using the *B3LYLP* functional as a perturbation on self consistent density with 6-31+G* basis set. The PESs were calculated with BSSE-corrected *MP2 6-31+G** level of theory. Basically, *MP2* is known to consistently provide a good description of intermolecular interactions [14]. These calculations have been carried out with a high accuracy large integration grid, so that sensitivity is minimized.

5. Biological activity

5.1. Cell culture

Cell lines were obtained from the American Type Culture Collection (ATCC) and the German Collection of Microorganisms and Cell Cultures (DSMZ). All cell lines were cultured under the conditions recommended by their respective depositors. Media were purchased from Sigma and Fetal Bovine Serum (FBS) was supplied by Invitrogen.

5.2. Cell proliferation assay

Growth inhibition was measured in 96-well plates. Aliquots of 120 μL of the suspended cells (5×10^4 Cells/mL) were given to 60 μL of compound solutions. After 5 days, growth was determined using MTT assay [15].

5.3. Mosquito culture

Cx. pipiens larvae were obtained from an in-house maintained colony and reared indoor at 27 ± 2 °C of 50 ± 5% relative humidity with 14:10 h/day of light:dark period. The emergent adults were fed with a 10% glucose solution in a jar with cotton wick. The

Table 1
Crystallographic data and refinement details for compounds **1, 6** and **13**.

	1	**6**	**13**
Formula	$C_{16}H_{11}N_3O_3S$	$C_{15}H_{10}N_4O_3S$	$C_{12}H_{11}NO_4S$
Formula weight	325.35	326.34	265.29
Crystal system	Monoclinic	Triclinic	Monoclinic
Space group	$P2_1/a$	P-1	$P2_1/a$
a (Å)	8.0778(9)	7.3199(7)	15.2735(16)
b (Å)	14.5640(14)	7.8798(7)	5.5502(6)
c (Å)	12.8205(12)	13.3033(12)	16.0039(16)
α (°)	90	72.163(2)	90
β (°)	99.879(3)	86.170(2)	114.376(3)
γ (°)	90	89.228(3)	90
V (Å^3)	1485.9(3)	728.79(12)	1235.7(2)
Z	4	2	4
D (calc) (g/cm^3)	1.454	1.487	1.426
θ Min–Max (°)	3.1, 27.5	3.1, 27.5	3.1, 27.5
Dataset (h; k; l)	−10:10; −18:17; −16:16	−9:9; −10:10; −16:17	−19:19; −7:7; −20:20
Tot., Uniq. Data, R(int)	17102, 3407, 0.048	7304, 3203, 0.027	12776, 2789, 0.052
Observed data ($I > 2.0\ \delta(I)$)	2144	2027	1973
Nref, Npar	3407, 209	3203, 209	2789, 164
R, wR_2, S	0.0420, 0.1588, 1.00	0.0426, 0.1703, 1.06	0.0527, 0.1545, 1.05
Min. and Max. Resd. Dens.	−0.40, 0.22	−0.31, 0.24	−0.30, 0.20

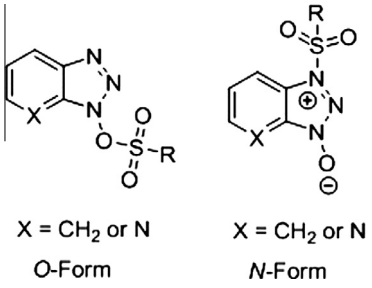

Fig. 2. The *O*- and *N*- forms of sulphonate active ester.

Table 2
Selected bond distances (Å) and angles (°) for compounds **1, 6** and **13**.

1			
S1–O1	1.4238(2)	N2–N3	1.306(4)
S1–O2	1.4108(2)	O1–S1–O2	122.31(15)
S1–O3	1.6803(2)	O1–S1–O3	100.19(13)
S1–C10	1.743(2)	O1–S1–C10	110.87(13)
O3–N1	1.380(2)	O2–S1–O3	106.76(12)
N1–N2	1.351(3)	O2–S1–C10	110.75(13)
N1–C11	1.360(3)	O3–S1–C10	103.65(10)
N2–N3	1.300(3)	S1–O3–N1	113.35(13)
N3–C16	1.388(3)	O3–N1–N2	120.2(2)
O1–S1–O2	122.12(11)	O3–N1–C11	126.9(2)
O1–S1–O3	105.74(9)	N2–N1–C11	111.5(2)
O1–S1–C10	111.19(10)	N1–N2–N3	107.6(2)
O2–S1–O3	99.94(11)	**13**	
O2–S1–C10	111.75(10)	S1–O1	1.416(2)
O3–S1–C10	103.52(9)	S1–O2	1.4201(19)
S1–O3–N1	113.22(12)	S1–O3	1.6611(19)
O3–N1–N2	118.51(16)	S1–C7	1.744(3)
O3–N1–C11	128.15(16)	O3–N1	1.399(2)
N2–N1–C11	12.66(17)	O4–C12	1.219(3)
N1–N2–N3	107.18(18)	N1–C8	1.366(4)
N2–N3–C16	108.43(19)	O1–S1–O2	122.45(12)
6		O1–S1–O3	102.06(11)
S1–O1	1.411(3)	O1–S1–C7	109.80(12)
S1–O2	1.418(2)	O2–S1–O3	108.28(10)
S1–O3	1.6671(18)	O2–S1–C7	109.87(12)
S1–C10	1.741(3)	O3-S1-C7	102.22(11)
O3–N1	1.370(3)	S1–O3–N1	114.55(15)
N1–N2	1.353(3)	O3–N1–C8	117.0(2)
N1–C11	1.367(3)	O3–N1–C12	115.83(19)
		C8–N1–C12	127.0(2)

adults were given mouse blood meals overnight. Glass Petri dish lined with filter paper and 100 mL tap water was kept inside the cage for ovi-position.

5.4. Larvicidal test

c. pipiens 4th instar larvae were tested with different concentrations of compound solutions. Each test solution was placed in 12 multi-well test plates along with the 4th instar larvae. Each experiment was conducted in triplicates and a concurrent control group was maintained. Dead larvae were counted after 24 h.

6. Results and discussion

The sulfonate esters were prepared by reaction of HOBt, HOAt, ethyl cyanoglyoxylate-2-oxime or 1-hydroxy-2-pryridinone with the sulfonyl chloride (toluene or naphthalene derivatives) using two phase DCM-H_2O method in presence of Na_2SO_4 to afford the corresponding sulfonate ester **1, 3, 6, 8, 11, 12** and **13** (Fig. 1). All prepared esters were characterized by ^1H and ^{13}C NMR spectra, giving similar data to those earlier reported [9,16]. As hypothesized from solution characterization, and derived from X-ray single crystal diffraction, the structures of the benzotriazole sulfonate esters showed that both esters are exist in *O*-form not *N*-form (Fig. 2).

In the molecular structures of **1**, **6** and **13,** the sulfur atoms adopt a variable distortion degree of tetrahedral geometry. In **1,** the dihedral angle between the best-fit least-square two planes of HOBt with naphthalene is 33.89(4)°. The same dihedral angle definition at **6** in-between HOAt and naphthalene is 49.79(5)°. The bridging C10-S1-O3-N1 sulfonate torsion angle is −67.63(1)° in **1,** 66.36(2)° in **6** and 102.13(2)° in **13**.

Selected bond distances with angles are presented in Table 2 and the molecular structures with thermal ellipsoidal numbering schemes for **1**, **6** and **13** are shown in Fig. 3.

In **1**, π–π interactions exist in between the naphthalene rings and HOBt part, with C–H···N hydrogen bonding of C(8) first level chain pattern along the *ac*-crystallographic plane. Fig. 4 and Table 3 presenting some highlights on the hydrogen bonding geometry featured in **1**, **6** and **13**, while for graph set descriptors, the readers are referred to [17].

In **6**, having a lower symmetry than **1** beside a clockwise rotation of the C10–S1–O3–N1 angle, the π–π interactions are no longer exist and only dimeric molecules are arranged with respect to

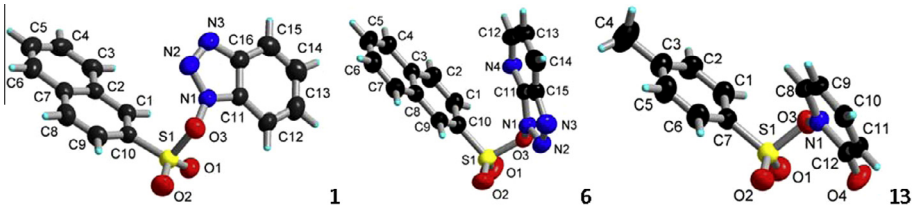

Fig. 3. Atomic numbering scheme of **1**, **6** and **13** displacement ellipsoids shown at 50% probability level.

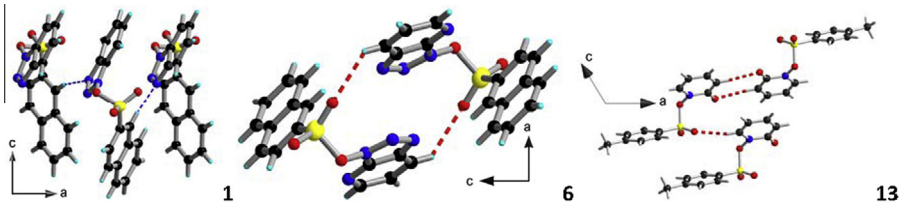

Fig. 4. Perspective drawing of the structures in **1**, **6** and **13** showing the intermolecular C–H···N and C–H···O hydrogen bonding. The C–H···N in **1** and the C–H···O hydrogen bonding in **6** with **13** are represented as blue and red dotted lines, respectively. For symmetry codes, see Table 3.

Table 3
Hydrogen bonding geometries for compounds **1**, **6** and **13**.

D-H···A	d(H···A)	d(D···A)	<(DHA)
1			
C1–H1···N3^{i}	2.48	3.387(3)	165
i: −1/2 + *x*, 3/2 − *y*, *z*			
6			
C14–H14···O2^{i}	2.60	3.345(4)	138
i: 1 − *x*, −*y*, −*z*			
13			
C8–H8···O2^{i}	2.43	3.342(3)	166
C11–H11···O4^{ii}	2.38	3.307(3)	173
i: *x*, −1 + *y*, *z*, ii: −*x*, 1 − *y*, 1 − *z*			

C–H···O hydrogen bond. In **13**, the ketonic (O4) is incorporated in dimeric C–H···O interactions.

In order to evaluate the energetic differences and similarities between hydrogen bonding in **1**, **6** and **13**, we carried out geometry optimizations, molecular electronic density and electrostatic density potentials calculations. The difference in molecular geometries, excluding hydrogen atoms, between the two *z*-matrices of single-crystal and geometry-optimized atomic coordinates in **1**, **6** and **13** was examined by structural overlay analyses using sulfonate SO_2 center. The overlay presented in Fig. 5 showed the r.m.s. deviation of 0.171, 0.099 and 0.074 Å in **1**, **6** and **13** respectively, with a clear effect of replacing HOBt with HOAt in **1** and **6**.

Fig. 5. Structural overlays of single crystal *vs. HF*-geometry optimized atomic coordinates in **1** (left), **6** (middle) and **13** (right).

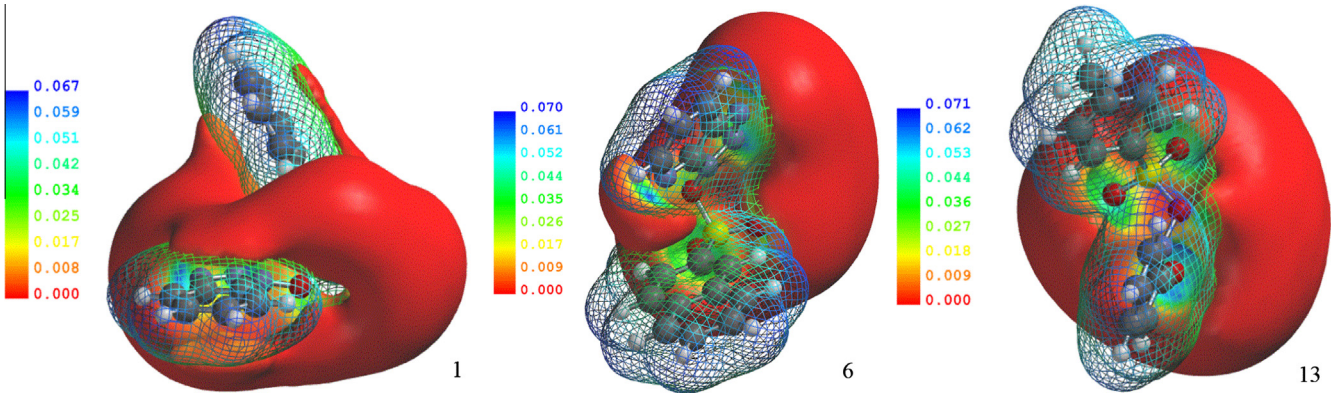

Fig. 6. electronic density isosurfaces (mesh in grey) and isoelectrostatic potentials (solid in red) for **1**, **6** and **13** calculated by *DFTMP2*. Isoelectrostatic surfaces are in the range +10 eV to −10 eV. Scales for electrostatic potentials are given in kJ/mol.

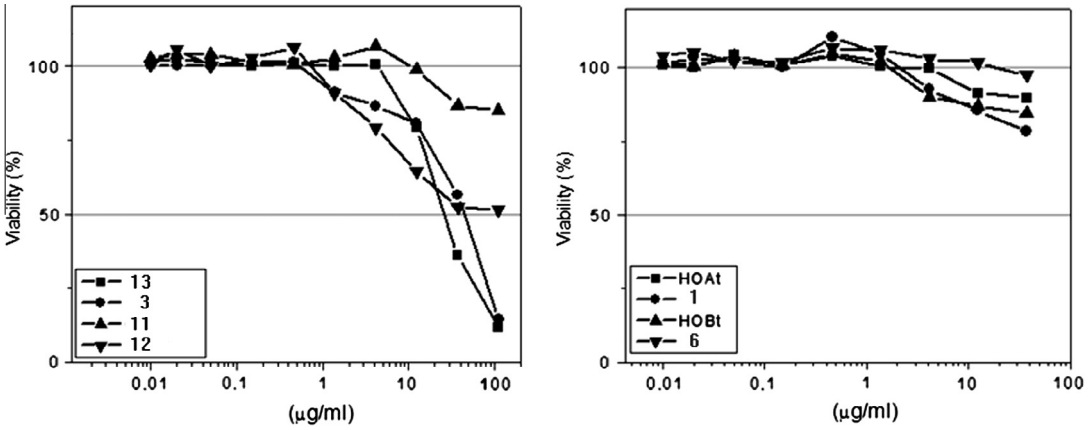

Fig. 7. Effect on the growth of colon human cancer cell line SW756.

Table 4
Larvicidal activities of tested compounds against 4th instar larvae of *cx. pipiens*. Mortality is given as mean ± e.s.d.%, and control with Nil mortality.

Compound	Concentration (μg/mL)						
	500	250	125	62.5	31.25	15.63	7.81
1	100 ± 0	40.33 ± 3.33	16.67 ± 3.33	0	0	0	0
11	100 + 0	40.33 ± 3.33	16.67 ± 3.33	0	0	0	0
12	100 ± 0	100 ± 0	100 ± 0	100 ± 0	40.33 ± 3.33	10 ± 0	0

The Møller–Plesset second level perturbation theory (*MP2*) is computationally – affordable *ab-initio* quantum calculation with *s*- and *p*-closed shell orbital of reasonable size organic molecules [18]. The restricted *MP2* correlation-corrected density matrix converges at energy slightly higher than SCF gradient. Fig. 6 depicts the isosurfaces of electronic density and electrostatic density potential. In **1** and **6,** the highest negative electronic density or the lowest delocalization parameter is defined around the triazole N-atom (N3) with less contribution from the sulfonyl O-atoms (O1 and O2). An evidence for the π–π interactions can be seen at PESs of **1**. In **13**, the negative electronic density is located mainly at the ketonic O-atom (O4). The electrostatic density potential is intensively localized at the C–H···N hydrogen-bonding acceptor atoms in **1**. In **6**, the energy associated with the C–H···N is greater than those of C–H···O hydrogen bond, while in **13** it is defined only at the C–H···O acceptor, as no C–H···N exists, with the greater contribution is at the ketone oxygen atom. Moreover, energy of the π–π interactions **1** can be seen as almost negligible, compared to those associated with the C–H···N hydrogen bonding.

To test possible anti-proliferation effects of the compounds, MTT-assay was performed according to a reported method [15]. Three cell lines were tested: the mouse fibroblast L929, the human cervices carcinoma cell line KB-3.1, and the human colon cancer cell line SW756. A constant number of cells were incubated with a serial dilution of each substance for 5 days under cultivation conditions as described in the method section. Methanol was used as a negative reference. The viability of the treated cells was calculated as a percent of the control cells. Fig. 7 shows the effect of the eight selected compounds on the growth of the SW756 cancer cell line. Only compounds **3** and **13** showed moderate anti-proliferative activities with IC_{50} – values of 50 and 25 μg/mL respectively, (Fig. 7 left). A weak anti-proliferative activity could be also observed with **12**, but the IC_{50} was undetermined. The rest of compounds showed no activities (Fig. 7 right). Similar results could be obtained with the two other cell lines.

We further investigated the effect of eight compounds on the larval development of *Cx. pipiens* 4th instar larvae. The laervae were incubated overnight with different concentration of the eight selected compounds (7.81–500 μg/mL). As shown in Table 4, only three out of the eight tested compounds were showing a larvicidal effect at microgram level concentration. Compound **1** and **11** inhibit the 4th instar larvae growth completely at concentration of 500 μg/mL. The inhibitory effect became around 40% at concentration of 250 μg/mL. In contrast, the larvicidal effect of **12** was stronger. This derivative fully inhibits the development of the larvae at 62.5 μg/mL. Further investigations are currently carried out in order to define the mechanism of larvae growth inhibition by these compounds.

To summarize, we present here the molecular structures X-ray single-crystal elucidation for three new sulfonate ester derivatives. We studied the intermolecular interactions in *DFT* geometry-optimized structures and evaluated the synthesized compounds against human cancer cells as well as mosquito. One of the tested compound was able to effectively inhibits the growth at relatively low concentration.

Acknowledgment

Authors are thankful for Mr. Almohannad Baabbad and the bio-products research chair at zoology department KSU for technical assistance.

Appendix A. Supplementary material

Supplementary data associated with this article can be found, in the online version, at http://dx.doi.org/10.1016/j.molstruc.2013.04.025.

References

[1] B. Kundu, S. Shukla, M. Shukla, Tetrahedron Lett. 35 (1994) 9613.
[2] S.K. Khare, G. Singh, K.C. Agarwal, B. Kundu, Protein Pept. Lett. 5 (1998) 171.
[3] L.A. Carpino, A. El-Faham, F. Albericio, Tetrahedron Lett. 35 (1994) 2279.
[4] N.B. Palakurthy, B. Mandal, Tetrahedron Lett. 52 (2011) 7132.
[5] A. El-Faham, F. Albericio, Chem. Rev. 111 (2011) 6557.
[6] D.Y. Zhang, Y.H. Ye, Peptide: Biology and Chemistry, Proceedings of the Chinese Peptide Symposium, Science Press, Beijing, China, 1991. 235.
[7] K.D. Wehrstedt, P.A. Wandrey, D. Heitkamp, J. Hazard. Mater. 126 (2005) 1.
[8] S.N. Khattab, Chem. Pharm. Bull 58 (2010) 501.
[9] L.A. Carpino, J. Xia, C. Zhang, A. El-Faham, J. Org. Chem. 69 (2004) 62.
[10] Crystal Clear, Rigaku, New Trails Dr., The Woodlands, TX, USA, 2009.
[11] G.M. Sheldrick, Acta Cryst. A64 (2008) 112.
[12] Diamond, Crystal Impact GbR version 3.1e, Bonn, Germany, 2007.
[13] SPARTAN08, Wavefunction 18401 Von Karman Avenue, Suite Irvine, CA 92612, USA, 2009.
[14] J.E. Del Bene, Encyclopedia of computational chemistry, vol. 1, Wiley, Chester, England, 1998. 1263.
[15] T. Mosmann, J. Immunol. Methods 65 (1983) 55–63.
[16] S.Y. Kim, N. Sung, J. Choi, S.S. Kim, Tetrahedron Lett. 40 (1999) 117.
[17] J. Bernstein, R.E. Davis, L. Shimoni, N.L. Chang, Angew. Chem. In. Ed. 34 (1995) 1555.
[18] C.J. Cramer, Essentials of Computational Chemistry; Theories and Models, second ed., Wiley, UK, 2004. 221.